Volume 1 | Number 1 | Jan 2013 | Pages 1–100

Journal of
Materials Chemistry A

Materials for energy and sustainability
www.rsc.org/materialsA

Li⁺

ROYAL SOCIETY
OF CHEMISTRY

ROYAL SOCIETY
OF CHEMISTRY

www.rsc.org/materialsA

PAPER

Plasma-grown graphene petals templating Ni-Co-Mn hydroxide nanoneedles for high-rate and long-cycle-life pseudocapacitive electrodes†

Guoping Xiong,[a,b] Pingge He,[a,b,c] Lei Liu,[c] Tengfei Chen[c] and Timothy S. Fisher*[a,b]

Ni-Co-Mn triple hydroxide (NCMTH) nanoneedles were coated on plasma-grown graphitic petals (GPs) by a facile one-step hydrothermal method for high-rate and long-cycle-life pseudocapacitive electrodes. Structural and compositional characteristics of NCMTHs indicate that the multi-component metal elements distribute homogeneously within the NCMTHs. Comparison of the electrochemical performance of the three-dimensional NCMTH electrodes to Ni-Co double hydroxides reveals that a synergistic effect of the hierarchical structure of GPs and NCMTHs enables their high rate capability and long cycle life. The NCMTH electrode maintains over 95% of its capacitance at a high charge/discharge rate of 100 mA cm^{-2} relative to its low-current (1 mA cm^{-2}) capacitance; and it exhibits very high specific capacitance of approximately 1400 F g^{-1} (based on the mass of NCMTH), high specific energy density ($\approx$ 30 Wh kg^{-1}) and power density ($\approx$ 39 kW kg^{-1}) at a high current density of 100 mA cm^{-2}, and excellent long-term cyclic stability (full capacitance retention over 3000 cycles). To assess functional behavior, two-terminal asymmetric supercapacitor devices with NCMTHs on graphitic petals as positive electrodes were assembled and tested to reveal ultrafast charge/discharge rates up to 5,000 mV s^{-1} (approx. two orders of magnitude faster than conventional asymmetric devices based on metal hydroxides) with high rate capabilities, and excellent long-term cyclic stability (full capacitance retention over 10,000 cycles).

1. Introduction

With growing energy demand and the looming depletion of fossil fuels, renewable electrochemical energy storage systems are under aggressive development in academic and industrial communities to satisfy current and future energy needs.[1] Among these energy storage systems, supercapacitors have attracted extensive attention because of their fast power delivery, long cycle life and low maintenance costs, making them promising to complement or even replace batteries as power supplies.[1,2] For practical applications, high rate capability and long cycle life are essential to achieve high-power, durable supercapacitors with suitable energy density.[3] In particular, nanomaterials have been commonly adopted to improve the rate capability of electrodes because of their short diffusion lengths;[4,5] this attribute of nanostructured electrodes is the focus of the present work, which reports the

detailed electrochemical characteristics of unique metal hydroxide nanoneedles grown on three-dimensional (3D) graphitic nanopetals.

Pseudocapacitive electrode materials, particularly metal oxides/hydroxides containing transition metal elements (e.g., Ni, Co, Mn) that are endowed with rich redox states, can significantly improve energy densities compared to their carbon-based counterparts.[6-9] However, their rate capabilities and long-term cycle life are typically poor because of their relatively low electrical conductivity.[10-13] Consequently, high specific capacitances and energy densities can only be achieved at relatively low current densities (low charge/discharge rates), defeating the primary purpose of using a supercapacitor for high-rate charge/discharge applications.[3] To alleviate this problem, binary metal oxides/hydroxides such as spinel nickel cobaltite (NiCo$_2$O$_4$) and related hydroxides have recently been proposed as promising electrode materials because of their low cost, relatively high electrical conductivity, high electrochemical activity, elemental abundance, and low environmental impact.[14-19]

To further ameliorate the charge transfer efficiency and reduce internal resistance, much research has been dedicated to developing various templates for metal hydroxides. Apart from commonly used templates with relatively low surface area (e.g., Ni foam[11,12,19] and stainless steel[20]), many carbon-

[a] Birck Nanotechnology Center, Purdue University, West Lafayette, IN 47907, USA.
E-mail: tsfisher@purdue.edu
[b] School of Mechanical Engineering, Purdue University, West Lafayette, IN 47907, USA.
[c] State Key Laboratory of Powder Metallurgy, Central South University, Changsha 410083, China.
† Electronic Supplementary Information (ESI) available: [The detailed experimental procedures, EDX, XPS and additional SEM/TEM images].
See DOI: 10.1039/x0xx00000

based nanomaterials such as reduced graphene oxide and carbon nanotubes are frequently adopted as nanotemplates for these pseudocapacitive materials. However, fabricating such electrodes involves the use of binder and substrates/current collectors with a limited surface area; consequently, electrical conductivity, rate capability, energy density and long-term cycle life of electrodes are undermined,[8,14,21,22] as well as functional characteristics (e.g., flexibility, thermal limits) of the electrodes. Therefore, developing new templates with high conductivity and high surface area to fully exploit the excellent pesudocapacitive properties of metal hydroxides remains an open challenge.

Graphitic petals (GPs),[23,24] containing a few layers of graphene that grow roughly perpendicularly to a substrate over a large surface area through catalyst-free microwave plasma chemical vapor deposition (MPCVD), are promising candidates as high-surface-area, high-electrical-conductivity and binder-free nanotemplates for the highly pesudocapacitive metal hydroxide electrodes. GPs synthesized on various substrates have been shown to exhibit outstanding electrochemical performance as double-layer capacitor electrodes[25-31] and as nanotemplates for several pesudocapacitive materials in prior work.[8,23,32,33] A comprehensive and detailed overview of GP growth and applications in energy storage has been provided by Bo et al.[27]

However, to date, this electrically conductive and unique GP structure with sharp edges has not been systematically utilized as a nanoscale template to exploit the electrochemical properties of metal hydroxides. New research should seek to understand the role of unique sharp edge structures during the charge/discharge processes before they can be broadly utilized in industrial applications.

Meanwhile, in order to increase charge storage (energy density) further, extensive work has been dedicated to developing metal oxide and/or hydroxide composite electrodes in order to increase redox activity (or the density of electroactive sites).[15,16,34-37] However, many challenges arise with the constituents physically distributed in heterogeneous composites: i) the multi-step fabrication procedures of the composite electrodes are complicated and costly; ii) interfaces between the heterogeneous constituents may reduce electron transfer efficiency; iii) full utilization of the electroactive sites of the composite electrode materials is difficult to achieve. Consequently, multi-component (n ≥ 3, where n is the number of metal components) metal oxides/hydroxides with a homogeneous element distribution may circumvent the foregoing issues.

To date, little prior work has considered multi-component metal oxide electrodes,[38] and to the best of our knowledge no such multi-component metal hydroxide electrodes have been reported for pseudocapacitive electrodes nor combined with graphene-like materials to form flexible pseudocapacitive composite electrodes. Here, we report a facile and cost-effective approach to fabricate porous NCMTH nanoneedle

arrays on 3D CC/GP substrates as a binder-free flexible electrode for high-rate energy storage devices. The facile one-step hydrothermal process to prepare the hydroxide electrodes is easily controllable without subsequent annealing and promising for potential scalable fabrication. The porous NCMTH nanoneedles with a homogenous distribution of metal elements can increase the number of redox states and thus electroactive sites, thereby further boosting energy and power densities. 3D CC/GPs structures provide a highly conductive substrate with numerous sharp graphene edges, along with the sharp NCMTH nanoneedles, that can further enhance local electrolyte ion diffusion and thus increase the rate capability of the hybrid electrodes. The hybrid CC/GPs/NCMTH electrodes exhibit outstanding electrochemical results, as described in subsequent sections, which are attributed to the unique structure of GPs/NCMTHs and the synergistic effect of NCMTH nanoneedles and GPs.

2. Experimental

2.1 Synthesis of graphene nanopetals on carbon cloth:

Carbon cloth substrates (5×10 mm^2, Fuel Cell Earth type CCP), elevated 7 mm above a 55-mm-diameter Mo puck by ceramic spacers, were subjected to MPCVD conditions of H$_2$ (50 sccm) and CH$_4$ (10 sccm) as the primary feed gases at 25 Torr total pressure. The substrates were initially exposed to hydrogen plasma for approximately 2 min, during which the plasma power gradually increased from 300 to 550 W. The GP growth time was 15 min to ensure the CC substrates were fully covered by GPs. More details of the GP growth process are provided in ESI†.

2.2 Synthesis of NCMTH nanoneedles on CC/GPs:

1.455 g Co(NO$_3$)$_2$•6H$_2$O, 1.45 g Ni(NO$_3$)$_2$•6H$_2$O, 1.255 g Mn(NO$_3$)$_2$•4H$_2$O and 0.9 g urea were dissolved in 70 mL of deionized water at room temperature to form a light pink solution. The detailed hydrothermal procedures are provided in the ESI†. Briefly, CC/GP substrates were immersed in the precursor solution and transferred to an autoclave. The autoclave was kept at 135 ˚C for 90 min in an electric oven and subsequently cooled to room temperature in air naturally. The samples were washed many times and sonicated to remove excessive metal hydroxides on CC/GPs. After cleaning, the samples were dried in air at a temperature of 80 ˚C for 3 hrs. The mass of metal hydroxides was measured by the weight difference before and after the hydrothermal process using a microbalance with an accuracy of 1 μg. The areal mass density of the NCMTHs on CC/GP substrates is 0.6 mg cm^{-2}.

2.3 Material Characterization:

The surface morphology of electrodes was characterized by field emission scanning electron microscope (SEM, Hitachi S-4800). The structure and chemical composition of the electrodes were investigated characterized by transmission electron microscopy (TEM, Japan FEM-2100F) combined with energy-dispersive X-ray spectroscopy (EDX) mapping, X-ray photoelectron spectroscopy (XPS K-Alpha 1063, UK Thermo Fisher), X-ray diffraction (XRD, D/max 2550) and Raman spectroscopy (Xplora spectrometer,

Horiba Jobin Yvon Inc.). The Brunauer-Emmett-Telle (BET) surface area of the NCMTH nanoneedles was determined via nitrogen sorption measurement at 77K.

2.4 Electrochemical Measurements:

The electrochemical performance of electrodes was evaluated using a Gamry Echem Testing System, Gamry Instruments, Inc., USA. Electrochemical measurements were conducted in a three-electrode configuration at room temperature using 2 M KOH as electrolyte for pseudocapacitive electrodes. The CC/GPs/NCMTH substrate served directly as the working electrode. Pt mesh and standard calomel electrode (SCE) were used as the counter and reference electrodes, respectively. Electrochemical impedance spectroscopy (EIS) measurements were carried out with an AC perturbation amplitude of 5 mV in the frequency ranging from 1 MHz to 0.1 Hz. The asymmetric supercapacitor devices were electrochemically characterized in a two-electrode configuration cell in 2 M KOH aqueous electrolyte solution. The methods to calculate specific capacitances, energy and power densities are provided in ESI†.

3. Results and discussion

Scheme 1 illustrates the unique structure of NCMTH nanoneedles on CC/GP substrates. Macroscopically woven CC, with gaps between two adjacent carbon fibers ranging from several micrometers to tens of micrometers, provides a flexible and conductive 3D current collector and creates channels for fast and effective electrolyte ion transport with low internal resistance. The 3D CC substrate not only significantly increases the surface area but also serves as a nanotemplate with numerous sharp edges for the multi-component metal hydroxide. Moreover, these thin protruding GP edges significantly accelerate ion diffusion due to low energy barriers,[8,26,39] improve mechanical contact between the pesudocapacitive material and current collector by roughening the carbon fiber surfaces, and most importantly enhance charge transfer efficiency to fully exploit the excellent pseudocapacitive properties of the NCMTHs by providing a direct path for efficient electron transport.
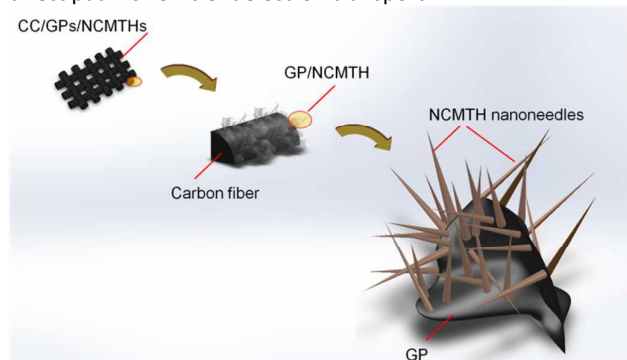
Scheme 1 Schematic illustration of the unique hierarchical structure of NCMTH nanoneedles on CC/GP substrates.

After a one-step microwave plasma growth process for 15 min (see details in ESI†, Fig. S1), GPs grow approximately 400 to 500 nm out from the carbon fiber surface, with a typical width of a single, unwrinkled 2D petal ranging from 100 nm to 400 nm and

a thickness of a few nanometers. These GPs are ultra-light, with an areal mass density of ≈ 1 mg cm^{-2}.Fig. 1a and 1b contain scanning electron microscopy (SEM) images of uniform NCMTH nanoneedles on CC/GP substrates. We note that by increasing the Mn content in the precursor solution, the morphology and structure of NCMTHs can be changed from nanoneedles to nanosheets (see details provided in ESI†, Figs. S2 and S3).As shown in Fig. 1a, NCMTHs grow homogenously on CC/GP substrates over a large scale (see Fig. 1a inset). The high-magnification image in Fig. 1b shows that the protruding NCMTHs with a nanoneedle shape generally grow perpendicularly to GP surfaces. These NCMTH nanoneedles exhibit ultra-sharp tips (diameters as small as a few nanometers) and lengths of hundreds of nanometers. For comparison, uniform and large-scale coverage of GPs without the NCMTHs on carbon fibers are shown in ESI†, Fig. S4.

As compared to relatively smooth GP surfaces (see ESI†, Fig. S4e), GPs/NCMTHs show distinct surface roughness and porosity, with sharp NCMTH nanoneedle tips and GP edges exposed (see Fig. 1b), which are beneficial to fast ion diffusion at high charge/discharge rates. A close-up of NCMTH nanoneedles on a single petal is shown in Fig. 1b inset, in which petal edges can be clearly distinguished. More SEM images of such unique structure of GPs/NCMTHs are shown in ESI†, Fig. S5. Notably, large channels (gaps between adjacent carbon fibers) created by the 3D CC substrate remain after the GP growth and NCMTH coating on the surface of carbon fibers, providing a prerequisite for fast ion diffusion rate (high rate capability). TEM and Raman characterization of GPs have been provided in ESI† Fig. S6 and Fig. S7, respectively. Notably, TEM characterization of GPs on carbon fibers in previous work[8,40] indicates that the fiber-petal transition occurs with crystalline continuity, which also promotes electron transport efficiency at the interface between carbon fibers and GPs, reduces internal resistance and thereby facilitates a high rate capability. Fig. 1c and 1d contain transmission electron microscopy (TEM) images of GPs/NCMTH nanoneedle structure. Fig. 1c displays many NCMTH nanoneedles decorating a GP. Needles with base diameters of tens of nanometers and tip diameters of a few nanometers are observed, in good agreement with the foregoing SEM results. The high-resolution TEM image in Fig. 1d reveals the porous structure of NCMTH nanoneedles (BET surface area of 55.2 m^2 g^{-1}), which facilitates electrolyte ion diffusion on/into the surface of the active pseudocapacitive material (enabling fast redox reactions) and further enhances charge storage in the electrodes by increasing the accessible surface area.

Energy dispersive X-ray spectrometry (EDX) elemental mapping images of GPs/NCMTH nanoneedles shown in Fig. 1e-1j reveal the spatial elemental distribution within the structure. Fig. 1e contains a high-angle annular dark field (HAADF) scanning TEM image of multiple NCMTH nanoneedles on a typical GP. Figs. 1f to 1j correspond to C, Co, Ni, Mn and O maps, respectively. These spatial elemental mappings not only confirm the unique structure of GPs/NCMTHs, but more importantly reveal a homogeneous spatial distribution of the mapped elements (Ni, Co, Mn and O) in the nanoneedle structure (see Fig. 1f-1j). The contents of the metal elements in the NCMTHs are estimated from the EDX elemental mapping and shown in ESI†, Table S1. The atomic ratio of Ni:Co:Mn:O in the NCMTH nanoneedles is estimated to be 5:5:1:20. We expect that the ratios can be tuned by adjusting the concentrations of raw chemicals in the precursor solution during the preparation process. The versatility of the preparation process of NCMTH nanoneedles can be demonstrated by growing these NCMTHs on a variety of substrates. For example, NCMTH nanoneedles grown on pure CC substrates are shown in ESI†, Fig. S8, in which the NCMTHs also display their ultra-sharp tips, similar to those grown on GPs.
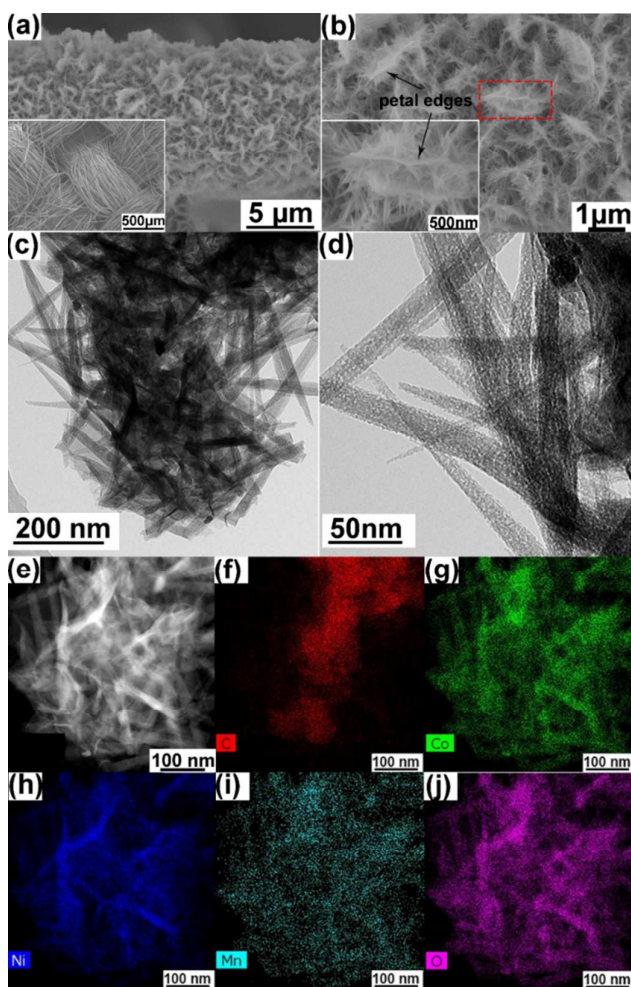
Fig. 1 (a) SEM image of CC/GPs/NCMTH nanoneedles at low magnification (the inset shows large-scale coverage of GPs/NCMTH nanoneedles on CC); (b) SEM image of CC/GPs/NCMTHs at high magnification (the inset indicates the petal edges from the red rectangular area). (c) TEM image of CC/GPs/NCMTHs; (d) High-resolution TEM image displaying the porous structure of NCMTH nanoneedles. (e) High-angle annular dark field (HAADF) scanning TEM image. (f-j) Elemental mapping showing uniform spatial distribution of mapped elements in the nanoneedles: (f) to (j) correspond to C, Co, Ni, Mn and O maps, respectively.

To investigate the crystallinity of NCMTHs, comparative XRD patterns of CC/GPs/NCMTH and CC/GPs/NCDHs (detailed preparation procedure provided in ESI†) are shown in Fig. 2a. As observed in both XRD patterns, the prominent peaks located at 26.4° and 44.4° correspond to graphite (002) and (101), respectively, and derive from CC/GP substrates. Because Ni and Co hydroxides possess similar structures, their diffraction peaks are similar and difficult to differentiate.[41] In the XRD pattern of CC/GPs/NCDHs, well-defined peaks located at 11.2° (001), 22.7° (002), 34° (100), and 59.6° (110) are due to the α-phase, and peaks at 32.55° (100), 38.95° (101) are due to the β-phase.[20] As estimated from the EDX analysis, the content of Mn in the triple-component metal hydroxide is much lower than that of Ni or Co. Moreover, $M(OH)_2$ (M= Ni, Co, Mn) generally possesses a similar

structure for different M;[42,43] therefore adding Mn will likely not change the crystal structure of the hydroxide significantly.[42,43] In the XRD pattern of CC/GPs/NCMTHs, relative intensities of foregoing peaks have changed to some extent, and some new peaks appear (indicated by the red labels in Fig. 2a), which might be attributed to the presence of Mn in the NCMTHs.

X-ray photoelectron spectroscopy (XPS) was employed to investigate the surface chemical composition of CC/GPs/NCMTHs, and full results are provided in ESI†, Fig. S9. The atomic percentage of metal elements in the NCMTHs based on XPS analysis is included in ESI, Table S2, in which the atomic percentages of Ni, Co and Mn in NCMTHs are 9.59%, 10.08% and 2.17%, respectively. The atomic ratio of Ni: Co: Mn is estimated as 5:5:1, which is consistent with the EDX results. Figs. 2b-2f contain detailed high-resolution XPS analyses of C 1s, O 1s, Ni 2p, Co 2p and Mn 2p, respectively. The C 1s spectrum in Fig. 2b can be fitted as four typical peaks, denoted as C1, C2, C3 and C4. Specifically, C1 at 284.6 eV indicates carbon atoms of C–C nonfunctional graphitic structures. C2 at 286.4 eV and C3 at 288.7 eV are attributed to C-O functional groups. C4 at 290.7 eV is the characteristic shakeup line of carbon in aromatic compounds.[44] In the O 1s spectrum (see Fig. 2c), three peaks O1, O2 and O3 have been fitted. The O1 at 529.2 eV is a typical peak of metal-oxygen bonds excellent long-term cycle life of the hybrid electrodes. The O2 at 531.6 eV and O3 at 533.2 eV are associated with C-O functional groups.[45] After NCMTH nanoneedle growth on CC/GPs, some covalent bonds form between C and O, suggesting that a robust bonding exists at the interface between the nanoneedles and GPs. This covalent bonding forms a strong basis for high charge transfer efficiency at the interface. The Ni 2p spectrum is fitted according to two spin-orbit doublets, characteristic of Ni^{2+} and Ni^{3+}, and two shakeup satellites (identified as "Sat.").[46] Similarly, the Co 2p spectrum is fitted with two spin-orbit doublets, characteristic of Co^{2+} and Co^{3+}, and two shakeup satellites.[46] The peaks in the Mn 2p spectrum at 641.5 and 653.2 eV correspond to Mn $2p_{3/2}$ and Mn $2p_{1/2}$, respectively. However, distinguishing the binding energies corresponding to the oxidation states of Mn^{2+} and Mn^{3+} is rather difficult.[47] Based on the XPS analysis, NCMTH nanoneedles possess a diverse composition of Ni^{2+}, Ni^{3+}, Co^{2+}, Co^{3+}, Mn^{2+} and Mn^{3+} on the surface, providing more electroactive sites than single- or double-component metal hydroxides. Raman spectroscopy was also used to characterize the structure of CC/GPs/NCMTHs, as shown in ESI†, Fig. S10.
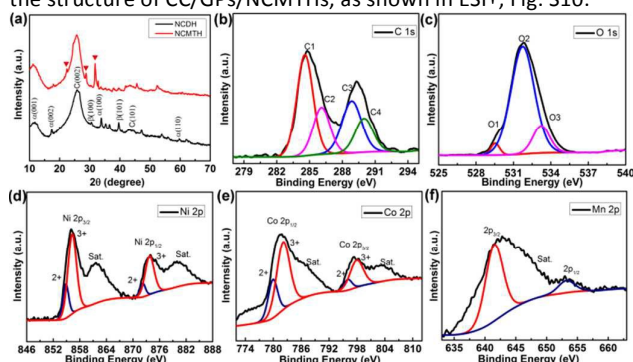

Fig. 2 (a) XRD pattern of CC/GPs/NCMTHs. High-resolution XPS spectra of (b) C 1s; (c) O 1s; (d) Ni 2p; (e) Co 2p; and (f) Mn 2p.

Fig. 3 contains results of the characteristic electrochemical performance of the hybrid electrodes. Fig. 3a shows typical

cyclic voltammetry (CV) profiles at scan rates from 5 to 100 mV s^{-1} with a potential window from −0.2 to 0.5 V vs. SCE for CC/GPs/NCMTH electrodes in 2 M KOH aqueous electrolyte. Two clear redox peaks appear in the CV curves corresponding to the redox reactions between NCMTHs and the alkaline electrolyte. Although detailed pseudocapacitive chemical pathways are not yet fully understood, plausible chemical processes associated with the behavior of NCMTHs follow:[48-51]
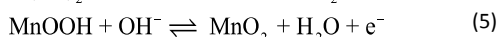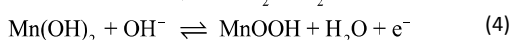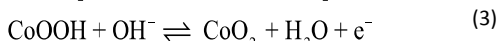
$$Ni(OH)_2 + OH^- \rightleftharpoons NiOOH + H_2O + e^- \tag{1}$$

$$Co(OH)_2 + OH^- \rightleftharpoons CoOOH + H_2O + e^- \tag{2}$$

$$CoOOH + OH^- \rightleftharpoons CoO_2 + H_2O + e^- \tag{3}$$

$$Mn(OH)_2 + OH^- \rightleftharpoons MnOOH + H_2O + e^- \tag{4}$$

$$MnOOH + OH^- \rightleftharpoons MnO_2 + H_2O + e^- \tag{5}$$

Fig. 3b provides galvanostatic charge/discharge profiles at different current densities ranging from 0.5 to 10 mA cm^{-2} (profiles at higher current densities from 12 to 100 mA cm^{-2} are shown in ESI†, Fig. S11). These constant-current charge/discharge curves display a relatively symmetric shape, which indicates high charge storage efficiency (coulombic efficiency) and reversible redox reactions. Voltage plateaus in discharge curves appear at around 0.2 V in the charge curves and 0.15 V in the discharge curves, which are consistent with the CV curves. The charge/discharge curves remain symmetrical even at current densities as high as 100 mA cm^{-2}, an indication of good high-rate stability.

For further comparison, CV curves of CC/GPs/NCMTH, CC/NCMTH and CC/GPs/NCDH electrodes at the same scan rate of 10 mV s^{-1} are plotted and shown in ESI† Fig. S12. Detailed CV curves of CC/NCMTH and CC/GPs/NCDH electrodes at different scan rates from 5 to 100 mV s^{-1} are shown separately in ESI†, Fig. S13. Comparative mass-based specific capacitances of CC/GPs/NCMTH, CC/ NCMTH and CC/GPs/NCDH electrodes calculated by the method described in the ESI† are plotted as a function of discharge current densities in Fig. 3c. Because the discharge curves in Fig. 3b indicate that the overwhelming majority of the capacitance derives from the pseudocapacitance of the transition metal hydroxides, the specific capacitances are normalized based on the mass of hydroxides. At a low current density of 1 mA cm^{-2}, CC/GPs/NCMTHs exhibit a specific capacitance of 1400 F g^{-1} (520 F g^{-1} based on the mass of GPs/NCMTHs and 65 F g^{-1} based on the total mass of CC/GPs/NCMTHs), approximately 2.3 and 2.7 times higher than those of CC/NCMTH and CC/GPs/NCDHs, respectively, and comparable to or typically higher than the reported values of conventional metal hydroxide-based pseudocapacitor electrodes.[16,17,20,51] The enhanced specific capacitance of the CC/GPs/NCMTH as compared to CC/GPs/NCDH electrodes corroborates the synergistic effects of Ni, Co and Mn in the metal hydroxides. The enhanced performance of CC/GPs/NCMTHs can also be attributed to the synergistic effect of GPs and the multi-component metal hydroxide. GPs here serve as a highly conductive template with high surface area, fully exploiting the pesudocapacitive properties of the multi-component metal hydroxide coating.[6,8]

Rate capability refers to the ability of the electrodes to retain capacity at high charge/discharge rates (high charge/discharge current densities), which is a critical parameter for supercapacitors that may limit their applicability in applications such as electric vehicles and hybrid electric vehicles. As indicated in Fig. 3c and 3d, specific capacitances of all three different electrodes show a gradual attenuation as the discharge current density increases. Fig. 3d plots the comparative rate capabilities of CC/GPs/NCMTH, CC/NCMTH and CC/GPs/NCDH electrodes, evaluated by calculating the capacitance retention as a function of discharge current densities from 1 to 100 mA cm^{-2}. Fig. 3d exhibits that the capacitance retention of CC/GPs/NCMTH electrodes reaches as high as 95.6% at a high current density of 100 mA cm^{-2} (equivalent to approximately 167 A g^{-1}) compared to that at 1 mA cm^{-2}, significantly higher than that of CC/NCMTH electrodes (79%) and slightly higher than that of CC/GPs/NCDH electrodes (94.8%).

These results are substantially better than the reported rate capabilities of the state-of-the-art single- and double-component metal hydroxides, which fall in the range of 40 to 80%.[16,18,36,52] (see ESI†, Table S3). Notably, the presence of GPs significantly increases the rate capability of the CC/GPs/NCMTH electrodes. The observed high rate capability can be primarily attributed to the large amounts of protruding GP sharp edges, the unique GP/NCMTH (edge-tip) structures, large surface area, binder-free fabrication process, high conductivity of GP templates coated with NCMTHs, and contiguous fiber-petal transition with crystalline continuity, since high rate capability is mainly determined by the kinetics of ion diffusion and electrical conductivity of the electrode materials.[5,53]
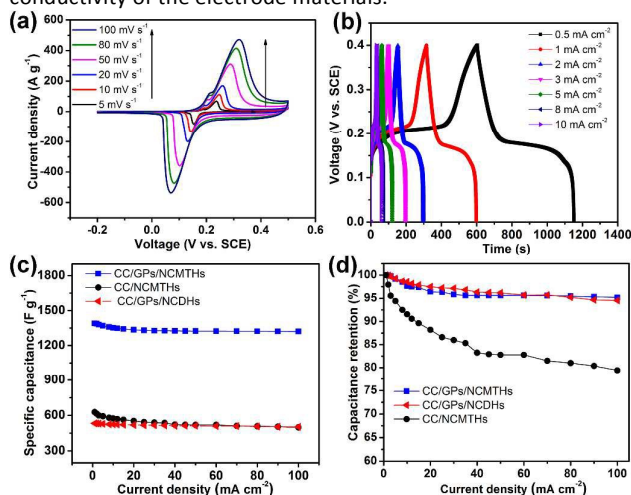

Fig. 3 (a) Cyclic voltammograms (CVs) of a CC/GPs/NCMTH hybrid electrode in a three-electrode cell with 2 M KOH aqueous solution at scan rates from 5 to 100 mV s^{-1}. (b) Galvanostatic charge/discharge curves of a CC/GPs/NCMTH hybrid electrode at low current densities from 0.5 to 10 mA cm^{-2} in the voltage range between 0 and 0.4 V vs. SCE. (c) Specific capacitances as a function of current density of a CC/GPs/NCMTH, CC/NCMTH and CC/GPs/NCDH hybrid electrodes. (d) Capacitance retention of a CC/GPs/NCMTH, CC/NCMTH and CC/GPs/NCDH hybrid electrodes.

A low equivalent series resistance is crucial to improve the electrochemical performance (e.g., maximum power density) of supercapacitor electrodes. Fig. 4a shows the Nyquist plot for the CC/GPs/NCMTH electrodes recorded from 0.1 Hz to 1 MHz. The measured impedance spectrum can be fitted by an equivalent circuit[54] consisting of a bulk electrolyte resistance Re, a charge transfer resistance R$_{ct}$, a pseudocapacitive element C$_p$ from

redox reactions of NCMTHs, and a constant phase element (CPE) to represent the double-layer capacitance (see Fig. 4a inset). Re is a combination of ionic resistance of the electrolyte, intrinsic resistance of the active material, and contact resistance at the interface between the active material and current collector.[55] Re can be obtained by calculating the real-axis intercept of the impedance spectrum at high frequencies. The Re value calculated from Fig. 4a for the CC/GPs/NCMTH electrodes is as low as 1.3 Ω. Charge-transfer resistance R_{ct}, known as Faradaic resistance, is a limiting factor for the specific power and rate capability of supercapacitors.[55] The semicircle in the high frequency region corresponding to charge transfer resistance R_{ct} is calculated to be 0.3 ohm − much smaller than observed in prior single- and double-component metal hydroxides.[13,20,56] This result suggests very low electrical resistivity of the CC/GPs/NCMTH electrode material, high diffusivity of the electrolyte ions through the pores, and high charge transfer efficiency at interfaces between the GPs/NCMTHs and electrolyte, leading to a high power and rate capability of the hybrid electrodes. The impedance measurements of the CC/NCMTH and CC/GPs/NCDH electrodes have been provided in ESI† Fig. S14.

As shown in the comparative Ragone plot (see Fig. 4b) for the CC/GPs/NCMTH, CC/NCMTH and CC/GPs/NCDH electrodes at different current densities, the CC/GPs/NCMTH electrode delivers an energy density of ≈30 Wh kg^{-1} at a power density of ≈39 kW kg^{-1}. On the other hand, CC/NCMTH and CC/GPs/NCDH electrodes exhibit energy densities of ≈11.5 Wh kg^{-1} at a power density of 37 kW kg^{-1} and ≈11.2 Wh kg^{-1} at a power density of 21 kW kg^{-1}, respectively. The energy density of CC/GPs/NCMTH decays slowly as the charge/discharge ratse increases because of a very high rate capability. The energy and power densities of CC/GPs/NCMTH electrodes are comparable or superior to those reported for different metal hydroxide electrodes at high current densities.[16,20,36,57]

Long-term cycle life for metal hydroxide electrodes, a crucial factor that affects their practical applications, remains a challenging issue.[9,13,16,20,53] Many possible factors such as mechanical detachment of the active materials from substrates, excessive volume expansion of active materials, low conductivity and limited mass transfer during charge/discharge processes may cause instability of the metal oxides/hydroxides over long-term cycling.[6,36] The cyclic stability of the 3D CC/GPs/NCMTH hybrid composite electrodes was evaluated at a current density of 10 mA cm^{-2} in the potential range of 0 to 0.4 V over 3000 cycles, as shown in Fig. 4c, in which specific capacitance retention is plotted as a function of cycle number. The 3D CC/GPs/NCMTH hybrid electrode exhibits 117% capacitance retention over 3000 charge/discharge cycles and high coulombic efficiencies (> 99%), indicating excellent long-term cyclic stability and high charge storage efficiencies. No noticeable changes in the morphology of the 3D CC/GPs/NCMTH hybrid electrode were observed after long-term cycling tests (see ESI†, Fig. S15). The excellent stability is likely attributable to the unique GPs/NCMTH structure (the robust mechanical contact between the nanoneedles and GPs), contiguous fiber-petal transition with crystalline continuity, and synergistic effect of the Ni, Co and Mn in this structure.

To further understand this phenomenon, long-term cyclic stabilities of CC/GPs/NCDH and CC/NCMTH electrodes were also tested under the same current densities over 3000 cycles (data are shown in ESI†, Fig. S16). Interestingly, similar to that of

CC/GPs/NCMTH electrodes, the capacitance of CC/NCMTH electrodes increases and then gradually stabilizes over 3000 charge/discharge cycles. This phenomenon of gradual increase of capacitance with cycle number has been observed for many metal oxide-containing electrodes in prior work and hypothetically explained by the gradually ameliorated electrolyte penetrating/wetting the electrodes and structural activation.[58-60] Likewise, CC/GPs/NCDH electrodes exhibit a gradual capacitance increase with cycle number over the first 100 cycles and then a steady capacitance loss appear over the remainder of the 3000 cycles with a capacitance loss of 5%. The enhanced long-term stability of the CC/GPs/NCMTH as compared to CC/GPs/NCDH electrodes corroborates the synergistic effects of Ni, Co and Mn in the metal hydroxides. Notably, the retention of CC/GPs/NCDH is still significantly higher than that reported in prior literature[20] and can be attributed to the synergistic effect of GPs and NCDHs.

The long-term cyclic stability tests suggest that NCMTH electrodes undergo more activation during the process of OH-insertion (extraction) during oxidation (reduction) than NCDH electrodes. Therefore, the excellent long-term stability is also likely attributable to the unique high-curvature characteristics of GPs/NCMTHs and possibly synergistic effects of the multi-component metal elements in the NCMTHs. Specifically, the unique needle-on-petal hierarchical structure not only enhances electrode contact area with the electrolyte but also accommodates the volume changes during thousands of charge/discharge cycles. More significantly, the synergic effect between GPs and NCMTHs may also inhibit the anodic dissolution of NCMTHs, and consequently improve the electrochemical reversibility and stability of the hybrid electrode. Multi-component NCMTHs with more electroactive sites may also be gradually exposed to the electrolyte upon repetitive charge/discharge cycling, leading to the observed gradual capacitance increase over thousands of cycles. A comparison of the cyclic stability of 3D CC/GPs/NCMTH hybrid electrodes to those of the state-of-the-art metal hydroxide electrodes has been provided in ESI†, Table S3.
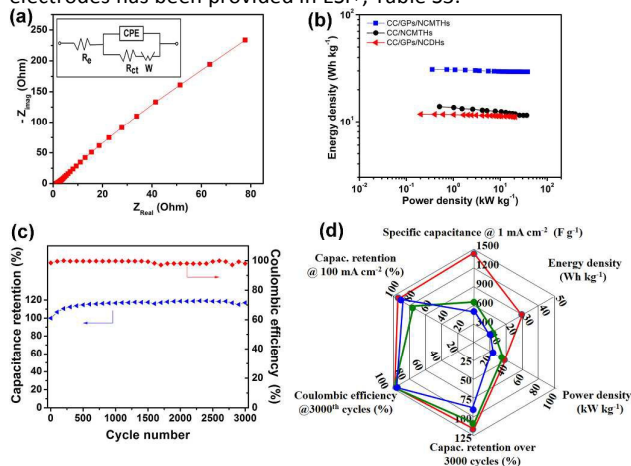

Fig. 4 (a) Nyquist plot for the NCMTH hybrid electrodes recorded from 0.1 Hz to 1 MHz. (b) Specific energy and power density (Ragone plot) of a CC/GPs/NCMTH, CC/ NCMTH and CC/GPs/NCDH hybrid electrodes evaluated at different charge/discharge rates (current densities). (c) Charge/discharge cyclic stability test at a current density of 10 mA cm^{-2} and coulombic efficiencies during the test. (d) A radar plot to

summarize the electrochemical performance of the CC/GPs/NCMTH (indicated by a red color), CC/NCMTH (green color) and CC/GPs/NCDH (blue color) hybrid electrodes.

The radar plot in Fig. 4d summarizes the overall electrochemical performance of 3D CC/GPs/NCMTH hybrid electrodes and compared to those of CC/GPs/NCDH and CC/NCMTH electrodes efficiently. Generally, a larger area encompassed within a radar plot indicates better overall electrochemical performance.[1] Fig. 4d indicates that the enclosed area within the red lines corresponding to CC/GPs/NCMTH hybrid electrodes is larger than those corresponding to CC/GPs/NCDH (blue color) and CC/NCMTH (green color) electrodes, respectively, corresponding to better overall electrochemical performance and warranting further development as a pseudocapacitive electrode material.

Because their electrochemical behavior, many metal oxide/hydroxide electrodes are classified as battery type materials.[3,61,62] Due to the formation of transition metal oxyhydroxides[61] during the charging process in an alkaline electrolyte, the multi-component metal oxide also fits this category. However, the battery-type behavior of these transitional metal oxides/hydroxides becomes increasingly pseudocapacitive with nanostructuring, leading to improved high-rate behavior due to a decrease in diffusion distances and, in some cases, the suppression of a phase transformation.[3,61,62] This type of material can be categorized with extrinsic pseudocapacitive materials.[3,61,62] As stated by Simon et al., such materials should be tested under the conditions that supercapacitors experience in field use.[3] In this work, CC/GPs/NCMTH hybrid electrodes exhibit high coulombic efficiencies (> 99%), ultra-fast ion kinetics (high rate capabilities) and long cycle life because of the nanoscale multi-component metal oxide coating on the high-surface-area graphene templates, enabling NCMTHs to exhibit high extrinsic pseudocapacitance at nanoscale dimensions.[3, 61, 62] Such battery-type materials with highly pesudocapacitive behavior that combine the high energy density of batteries along with the high power density and long cycle life of supercapacitors should be developed further into practical, scaled up technologies.[3]

To test the foregoing hypothesis that the hierarchical structure of GPs and NCMTHs promotes their high rate capability and long cycle life, we assembled asymmetric supercapacitor devices consisting of a chemically treated CC/GP negative electrode and a CC/GPs/NCMTH positive electrode and characterized their performance (detailed fabrication procedures are provided in ESI†). The electrochemical performance of two-terminal asymmetric supercapacitor devices (CC/GPs//CC/GPs/NCMTHs) in 2 M KOH aqueous electrolyte solution is shown in Fig. 5. The CV curves at relatively low scan rates from 100 mV s^{-1} to 1,000 mV s^{-1} shown in Fig. 5a display nearly ideal rectangular shapes, indicating a fast ion diffusion rate of these devices and a low internal resistance. The CV curves maintain nearly rectangular shapes, even at 5,000 mV s^{-1} (see Fig. 5b), which is almost two orders of magnitude faster than conventional metal hydroxide-based asymmetric supercapacitor devices.[9,17,37,50,63-65] The discharge current as a function of scan rate is plotted and shown in Fig. 5c, in which a linear dependence between the two is observed up to 5,000 mV s^{-1}, again indicating outstanding rate capability. As shown in ESI†, Fig. S17, CC/GPs//CC/GPs/NCMTH asymmetric supercapacitor devices exhibit a high capacitance retention of

approximately 75% at 1000 mV s^{-1} compared to that at 100 mV s^{-1}, suggesting a high rate capability, substantially better than those of metal hydroxide-based asymmetric supercapacitor devices, which fall in the range of 30% to 60% even at comparatively lower charge/discharge rates.[9,17,37,50,63-65] The high rate capability is also linked with low internal resistances in the device (see ESI†, Fig. S18). This result indicates that GP/NCMTH positive electrodes with high-curvature characteristics (e.g., sharp edges and tips) facilitate rapid access of electrolyte ions to the surfaces of electrodes with short ion diffusion length, leading to high charge/discharge rates.

Excellent long-term cycle life is crucial for asymmetric supercapacitor devices in practical applications. The cyclic stability of the as-prepared asymmetric supercapacitor devices was tested in the potential range of 0 to 1.4 V over 10,000 constant-current charge/discharge cycles at a current density of 8 mA cm^{-2}. As indicated in Fig. 5d, the device capacitance gradually increases with cycle number until the 6000th cycle (approx.), and then decreases steadily through the end of testing (10,000th cycle), with a capacitance retention of 114% compared to the first cycle, which is significantly better than state-of-the-art hydroxide-based asymmetric devices reported in prior work.[9,17,37,50,63-65] Notably, a capacitance increase during the cycling processes due to apparent activation of NCMTHs was also observed, consistent with the long-term cycling behavior of NCMTHs in a three-electrode configuration cell (see Fig. 4c and Fig. S16a). This phenomenon supports the notion that NCMTHs may undergo substantial activation during the charge/discharge processes many thousands of cycles, after which steady, slow capacitance loss appears. Coulombic efficiency gradually increases initially (95% in the first cycle) with cycle number and maintains high values (> 98%) through the 10,000th cycle, indicating high charge transfer efficiencies over long-term cycling. This set of results demonstrates the promising potential of applying 3D CC/GPs/NCMTHs as positive electrodes for high-rate and long-cycle-life asymmetric supercapacitor devices.
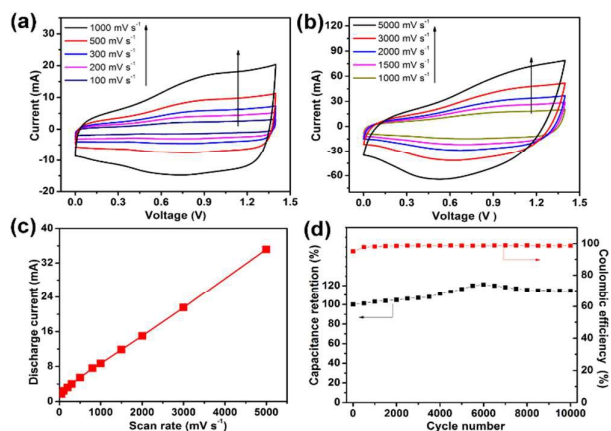

Fig. 5 The electrochemical performance of two-terminal asymmetric supercapacitor devices (CC/GPs//CC/GPs/NCMTHs) in 2 M KOH aqueous electrolyte solution. (a) CVs of CC/GPs//CC/GPs/NCMTH supercapacitor devices at scan rates from 100 to 1000 mV s^{-1} from 0 to 1.4 V. (b) CVs of CC/GPs//CC/GPs/NCMTH devices at scan rates from 1000 to 5000 mV s^{-1}. (c) Discharge current as a function of scan rate. (d) Charge/discharge cyclic stability test at a current density of 8 mA cm^{-2} and coulombic efficiencies during the test.

4. Conclusions

In summary, a nanoarchitecture based on a 3D CC/GPs/NCMTH hybrid has been prepared and investigated as a pseudocapacitive electrode. First, GPs were grown on CC substrates by MPCVD; second, NCMTH nanoneedles were coated on surface of GPs by a facile one-step hydrothermal approach. These hybrid pseudocapacitive electrodes exhibit high rate capability, high energy and power density, and excellent long-term cycle life in a three-electrode configuration cell, and show tremendous potential as high-rate and long-cycle-life positive electrodes for two-terminal asymmetric supercapacitor devices. The electrochemical performance of the pseudocapacitive electrodes can likely be improved in the future by optimizing factors such as the ratio of the multi-component metal elements in the NCMTHs and GP growth time. The present results suggest that the combination of well-anchored nanopetals on the versatile carbon cloth substrate with a new pseudocapacitive material is particularly well-suited for practical implementation as a high-rate, durable pseudocapacitive electrode. Moreover, the unique nanoarchitecture of the hybrid electrode may also be applicable to other electrochemical systems such as lithium ion batteries, fuel cells and non-enzymatic biosensors.
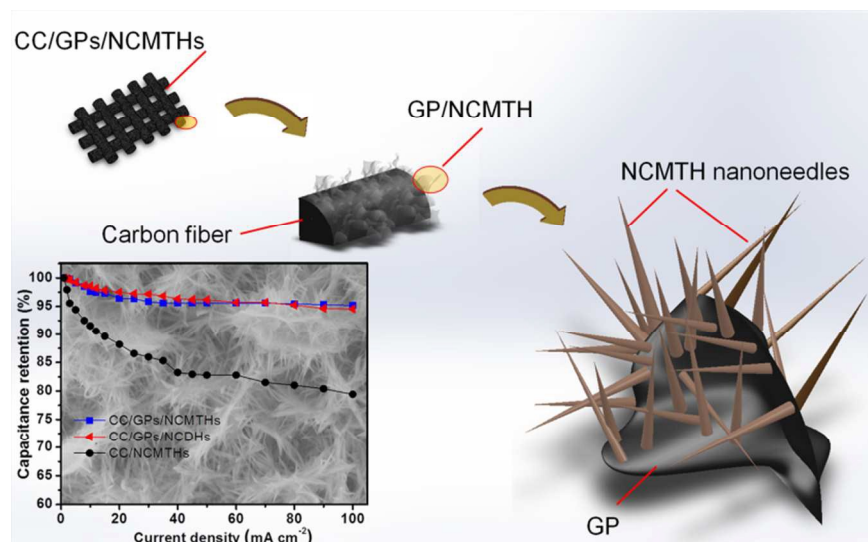
Acknowledgements

Notes and references

1   G. P. Xiong, C. Z. Meng, R. G. Reifenberger, P. P. Irazoqui and T. S. Fisher, *Electroanal.*, 2014, 26, 30-51.
2   P. Simon and Y. Gogotsi, *Nat. Mater.*, 2008, 7, 845-854.
3   P. Simon, Y. Gogotsi and B. Dunn, *Science*, 2014, 343, 1210-1211.
4   L. Taberna, S. Mitra, P. Poizot, P. Simon and J. M. Tarascon, *Nat. Mater.*, 2006, 5, 567-573.
5   H. Jiang, J. Ma and C. Z. Li, *Chem. Commun.*, 2012, 48, 4465-4467.
6   G. P. Xiong, K. P. S. S. Hembram, R. G. Reifenberger and T. S. Fisher, *J. Power Sources*, 2013, 227, 254-259.
7   X. Huang, X. Y. Qi, F. Boey and H. Zhang, *Chem. Soc. Rev.*, 2012, 41, 666-686.
8   G. P. Xiong, C. Z. Meng, R. G. Reifenberger, P. P. Irazoqui and T. S. Fisher, *Adv. Energy Mater.*, 2014, 4, 1300515.
9   J. Y. Ji, L. L. Zhang, H. X. Ji, Y. Li, X. Zhao, X. Bai, X. B. Fan, F. B. Zhang and R. S. Ruoff, *Acs Nano*, 2013, 7, 6237-6243.
10 M. J. Zhi, C. C. Xiang, J. T. Li, M. Li and N. Q. Wu, *Nanoscale*, 2013, 5, 72-88.
11 H. Jiang, T. Zhao, C. Z. Li and J. Ma, *J. Mater. Chem.,* 2011, 21, 3818-3823.
12 G. W. Yang, C. L. Xu and H. L. Li, *Chem. Commun.*, 2008, 48, 6537-6539.
13 T. Zhao, H. Jiang and J. Ma, *J. Power Sources*, 2011, 196, 860-864.
14 G. Q. Zhang, H. B. Wu, H. E. Hoster, M. B. Chan-Park and X. W. Lou, *Energ. Environ. Sci.*, 2012, 5, 9453-9456.
15 L. Yu, G. Q. Zhang, C. Z. Yuan and X. W. Lou, *Chem. Commun.*, 2013, 49, 137-139.
16 L. Huang, D. C. Chen, Y. Ding, S. Feng, Z. L. Wang and M. L. Liu, *Nano Lett.*, 2013, 13, 3135-3139.
17 X. Sun, G. K. Wang, H. T. Sun, F. Y. Lu, M. P. Yu and J. Lian, *J. Power Sources*, 2013, 238, 150-156.
18 M. Wang, J. Xue, F. Zhang, W. Ma and H. Cui, *J. Nanopart. Res.*, 2015, 17, 1-9.
19 J. Pu, Y. Tong, S. B. Wang, E. H. Sheng and Z. H. Wang, *J. Power Sources*, 2014, 250, 250-256.
20 R. R. Salunkhe, K. Jang, S. W. Lee and H. Ahn, *RSC Adv.*, 2012, 2, 3190-3193.
21 R. B. Rakhi, W. Chen, D. Y. Cha and H. N. Alshareef, *Nano Lett.*, 2012, 12, 2559-2567.
22 J. H. Kim, K. Zhu, Y. F. Yan, C. L. Perkins and A. J. Frank, *Nano Lett.*, 2010, 10, 4099-4104.
23 G. P. Xiong, K. P. S. S. Hembram, D. N. Zakharov, R. G. Reifenberger and T. S. Fisher, *Diam. Relat. Mater.*, 2012, 27-28, 1-9.
24 Y. H. Wu, B. J. Yang, G. C. Han, B. Y. Zong, H. Q. Ni, P. Luo, T. C. Chong, T. S. Low and Z. X. Shen, *Adv. Funct. Mater.*, 2002, 12, 489-494.
25 G. P. Xiong, C. Z. Meng, R. G. Reifenberger, P. P. Irazoqui and T. S. Fisher, *Energy Technol.*, 2014, 2, 897-905.
26 J. R. Miller, R. A. Outlaw and B. C. Holloway, *Science*, 2010, 329, 1637-1639.
27 Z. Bo, S. Mao, Z. J. Han, K. Cen, J. Chen and K. K. Ostrikov, *Chem. Soc. Rev.*, 2015, 44, 2108-2121.
28 X. Zhao, H. Tian, M. Y. Zhu, K. Tian, J. J. Wang, F. Y. Kang and R. A. Outlaw, *J. Power Sources*, 2009, 194, 1208-1212.
29 Z. Bo, Z. Wen, H. Kim, G. Lu, K. Yu and J. Chen, *Carbon*, 2012, 50, 4379–4387.
30 H.-F. Yen, Y.-Y. Horng, M.-S. Hu, W.-H. Yang, J.-R. Wen, A. Ganguly, Y. Tai, K.-H. Chen and L.-C. Chen, *Carbon*, 2015, 82, 124-134.
31 D. H. Seo, S. Yick, S. Pineda, D. Su, G. Wang, Z. J. Han and K. Ostrikov, *ACS Sustainable Chemistry & Engineering*, 2015, 3, 544-551.
32 C. Wang, J. Xu, M. F. Yuen, J. Zhang, Y. Li, X. Chen and W. Zhang, *Adv. Funct. Mater.*, 2014, 24, 6372-6380.
33 D. H. Seo, Z. J. Han, S. Kumar and K. Ostrikov, *Adv. Energy Mater.*, 2013, 3, 1316-1323.
34 J. X. Li, M. Yang, J. P. Wei and Z. Zhou, *Nanoscale*, 2012, 4, 4498-4503.
35 M. C. Liu, L. B. Kong, C. Lu, X. M. Li, Y. C. Luo and L. Kang, *ACS Appl. Mater. Inter.*, 2012, 4, 4631-4636.
36 H. Jiang, C. Z. Li, T. Sun and J. Ma, *Chem. Commun.*, 2012, 48, 2606-2608.
37 H. Chen, L. F. Hu, Y. Yan, R. C. Che, M. Chen and L. M. Wu, *Adv. Energy Mater.*, 2013, 3, 1636-1646.
38 J. M. Luo, B. Gao and X. G. Zhang, *Mater. Res. Bull.*, 2008, 43, 1119-1125.
39 C. Uthaisar and V. Barone, *Nano Lett.*, 2010, 10, 2838-2842.
40 T. Bhuvana, A. Kumar, A. Sood, R. H. Gerzeski, J. J. Hu, V. S. Bhadram, C. Narayana and T. S. Fisher, *ACS Appl. Mater. Inter.*, 2010, 2, 644-648.
41 V. Gupta, S. Gupta and N. Miura, *J. Power Sources*, 2008, 175, 680-685.

Journal of Materials Chemistry A Accepted Manuscript

Journal of Materials Chemistry A Accepted Manuscript

42 M.-H. Lee, Y.-J. Kang, S.-T. Myung and Y.-K. Sun, *Electrochim. Acta*, 2004, 50, 939-948.

43 S. Jouanneau and J. Dahn, *Chem. Mater.*, 2003, 15, 495-499.

44 S. Kundu, Y. M. Wang, W. Xia and M. Muhler, *J. Phys. Chem. C*, 2008, 112, 16869-16878.

45 J. F. Marco, J. R. Gancedo, M. Gracia, J. L. Gautier, E. Rios and F. J. Berry, *J. Solid State Chem*., 2000, 153, 74-81.

46 B. Cui, H. Lin, Y. Z. Li, J. B. Li, P. Sun, X. C. Zhao and C. J. Liu, *J. Phys. Chem. C*, 2009, 113, 14083-14087.

47 S. Bag, K. Roy, C. S. Gopinath and C. R. Raj, *ACS Appl. Mater. Inter*., 2014, 6, 2692-2699.

48 H. W. Wang and X. F. Wang, Acs Appl. Mater. Inter., 2013, 5, 6255-6260.

49 X. Wang, X. D. Han, M. Lim, N. Singh, C. L. Gan, M. Jan and P. S. Lee, *J. Phys. Chem. C*, 2012, 116, 12448-12454.

50 X. Wang, A. Sumboja, M. F. Lin, J. Yan and P. S. Lee, *Nanoscale*, 2012, 4, 7266-7272.

51 J. Gomez and E. E. Kalu, *J. Power Sources*, 2013, 230, 218-224.

52 W. Zhu, Z. Y. Lu, G. X. Zhang, X. D. Lei, Z. Chang, J. F. Liu and X. M. Sun, *J. Mater. Chem. A*, 2013, 1, 8327-8331.

53 Y. Hou, Y. W. Cheng, T. Hobson and J. Liu, *Nano Lett.*, 2010, 10, 2727-2733.

54 B. E. Conway, Electrochemical Supercapacitors: Scientific Fundamentals and Technological Applications, Kluwer-Plenum, New York, 1999.

55 J. Gamby, P. L. Taberna, P. Simon, J. F. Fauvarque and M. Chesneau, *J. Power Sources*, 2001, 101, 109-116.

56 M. F. Shao, F. Y. Ning, Y. F. Zhao, J. W. Zhao, M. Wei, D. G. Evans and X. Duan, *Chem. Mater.*, 2012, 24, 1192-1197.

57 C. C. Hu, J. C. Chen and K. H. Chang, J. Power Sources, 2013, 221, 128-133.

58 S. K. Meher and G. R. Rao, *J. Phys. Chem. C*, 2011, 115, 15646-15654.

59 X. J. Zhang, W. H. Shi, J. X. Zhu, W. Y. Zhao, J. Ma, S. Mhaisalkar, T. L. Maria, Y. H. Yang, H. Zhang, H. H. Hng and Q. Y. Yan, *Nano Res.*, 2010, 3, 643-652.

60 C. Z. Yuan, X. G. Zhang, L. H. Su, B. Gao and L. F. Shen, *J. Mater. Chem.*, 2009, 19, 5772-5777.

61 V. Augustyn, P. Simon and B. Dunn, *Energ. Environ. Sci*., 2014, 7, 1597-1614.

62 Y. Gogotsi and P. Simon, *Science Magazine*, 2011, 334, 917-918.

63 J. Yan, Z. Fan, W. Sun, G. Ning, T. Wei, Q. Zhang, R. Zhang, L. Zhi and F. Wei, *Adv. Funct. Mater*., 2012, 22, 2632-2641.

64 Z. Tang, C. H. Tang and H. Gong, *Adv. Funct. Mater*., 2012, 22, 1272-1278.

65 J. W. Lang, L. B. Kong, M. Liu, Y. C. Luo and L. Kang, *J. Solid State Electr.*, 2010, 14, 1533-1539.

Journal of Materials Chemistry A Accepted Manuscript

Ni-Co-Mn triple hydroxide (NCMTH) nanoneedles were coated on plasma-grown graphitic petals (GPs) by a facile one-step hydrothermal method for high-rate and long-cycle-life pseudocapacitive electrodes.